Institution of MECHANICAL ENGINEERS

Journal of ENGINEERING IN MEDICINE

An in vitro approach to the evaluation of foot-ankle kinematics: Performance evaluation of a custom-built gait simulator

Koen Peeters[1], Tassos Natsakis[1], Josefien Burg[1], Pieter Spaepen[2], Ilse Jonkers[3], Greta Dereymaeker[1] and Jos Vander Sloten[1]

Abstract

Despite their well-known limitations, in vitro experiments have several benefits over in vivo techniques when exploring foot biomechanics under conditions characteristic of gait. In this study, we present a new setup for dynamic in vitro gait simulation that integrates a numerical model for generating the tibial kinematics control input, and we present an innovative methodology to measure full three-dimensional joint kinematics during gait simulations. The gait simulator applies forces to the tendons. Tibial kinematics in the sagittal plane is controlled using a numerical model that takes into account foot morphology. The methodology is validated by comparing joint rotations measured during gait simulation with those measured in vivo. In addition, reliability and accuracy of the control system as well as simulation input and output repeatability are quantified. The results reflect good control performance and repeatability of the control inputs, vertical ground reaction force, center of pressure displacement, and joint rotations and translations. In addition, there is a good correspondence to in vivo kinematics for most patterns of motion at the ankle, subtalar, and Chopart's joints. Therefore, these results show the relevance and validity of including specimen-specific information for defining the control inputs.

Introduction

Three approaches are commonly used to investigate foot and ankle biomechanics, that is, examination of live subjects, manipulation of mathematical models, and in vitro experimentation.[1] Each of these methods contribute to our current understanding of foot and ankle biomechanics. However, in vitro experimentation has specific benefits over other methods, as they allow complete access to all tissues of the foot.[2] Hence, the effect of subsequent dissections or manipulations of the structures on foot biomechanics can be explored. Moreover, as all applied forces can be fully controlled, high repeatability of the testing conditions can be achieved.

In order to investigate foot function under dynamic conditions representative of gait, several groups have developed a setup for dynamic in vitro gait simulation using cadaveric feet,[1,3–7] all applying forces to the tendons and controlling tibial kinematics, in some cases supplemented with ground reaction forces. Since the first publication on in vitro gait simulation,[1] each group has focused on improving several aspects of the existing approaches, being mainly the limited degrees of freedom of the mechanism controlling the kinematics of the tibia, the low gait speed, the limited forces applied to the tendons, and the limited ground reaction force magnitudes. In the most recent simulators, most of

[1]Biomechanics Section, Mechanical Engineering Department, Faculty of Engineering KU Leuven, Belgium
[2]Katholieke Hogeschool Kempen, Geel, Belgium
[3]Human Movement Biomechanics Section, Department of Kinesiology, KU Leuven, Belgium

Corresponding author:
Koen Peeters, Biomechanics Section, Mechanical Engineering Department, KU Leuven Celestijnenlaan 300C, P.O. Box 2419, 3001 Heverlee, Belgium.
Email: koen.peeters@mech.kuleuven.be

these targeted improvements were achieved,[6,7] thereby improving the validity of simulation results and their relevance for clinical practice. However, some drawbacks remain. One is the lack of specimen specificity of the inputs to the control mechanism, namely, the forces applied to the tendons, ground reaction forces, and tibial kinematics. Therefore, in vitro experimentation still relies to a large extent on arbitrary and manual tuning of the control inputs and observer-dependent evaluation of the simulation results. This inevitably undermines standardization of the simulation procedure and potentially limits the reproducibility of the simulator performance over different specimens.

In this work, we first present a new setup and measurement protocol for dynamic in vitro gait simulations together with a strategy to reconstruct complete three-dimensional (3D) joint kinematics from the collected raw data. Next, we evaluate our innovative approach by presenting the reliability and accuracy of the control system (hereafter referred to as control performance), the repeatability of the inputs to the control system, the repeatability of the simulated kinematics and kinetics, and the correspondence of gait kinematics and kinetics to in vivo.

The setup uses a unique method for generating the tibial kinematics control input, based on a numerical model for knee and ankle motion in the sagittal plane, accounting for the specimen morphology.[8] This methodology eliminates the need for arbitrary tuning of the tibial kinematics input to the control mechanism for each individual specimen compared with existing approaches. Furthermore, it solves the problem of generating good tibial kinematics control inputs for simulations with feet, having rather extreme dimensions.[1,7] The strategy to calculate 3D joint kinematics allows to calculate joint translations in addition to rotations commonly reported in literature.[9–14] Therefore, it combines computed tomography (CT) data with data from a 3D motion capture device. This allows us to calculate and visualize bone motion in the global reference frame and, as such, to provide the reader with data for profound validation of numerical models of the hindfoot[15] and for validation of other in vitro experiments or in clinical studies that focus on understanding pathological hindfoot kinematics.

Methods and materials

Specimen preparation

Six freshly frozen cadaveric feet, all donated for scientific research, were tested in the gait simulator (Figure 1). A surgeon exposed the tendons of all extrinsic muscles and dissected the muscle belly from the tendons, leaving muscle lines of action and other ankle structures intact. Intracortical titanium pins, 4 mm in diameter and 50 mm in length (ICOS, Newdeal, France), were inserted in the tarsal bones (talus, calcaneus, cuboid, navicular) and the tibia. Their rotation was blocked by a stabilizing device and by inserting a two-component epoxy resin in the bone cavity (Pattex SuperMix Universal 5 min, NV Henkel, Belgium). The stabilizing device consists of a hollow tube with three nails protruding from one end. The device was first nailed on the bone, and the pins were inserted next through the tube and fixed to it with a screw. Their position in the bones was verified using 0.5-mm resolution spiral CT (Aquillion 64, Toshiba Medical Systems B.V., Japan). After preparation, feet were stored in a freezer (-18 °C) and defrosted in a temperature controlled room (18 °C) overnight before testing. Relevant dimensions of all feet, relevant for defining the control inputs to our setup, are displayed in Table 1.
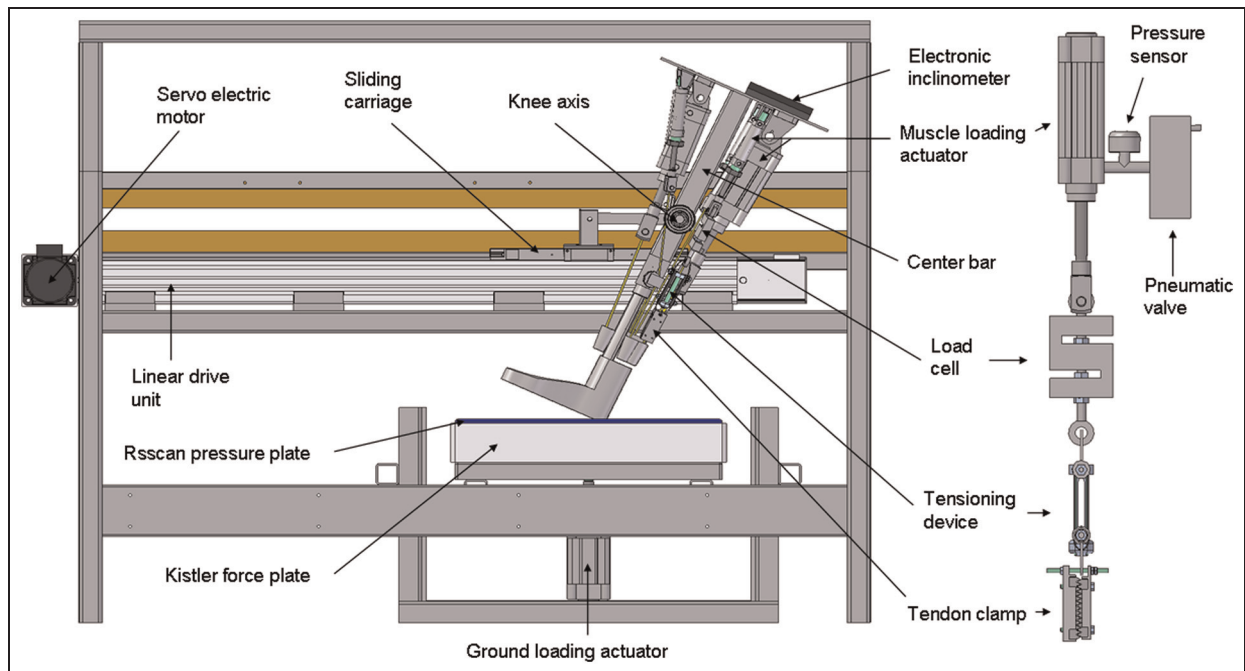
Gait simulator

The gait simulator consists of a framework (ITEM Industrietechnik GmbH, Germany). This framework carries a frame that bears six pneumatic actuators (Festo AG & Co. KG, Germany), each applying loads to the tendons of a cadaveric foot (Figure 2). The foot is mounted in the simulator by the bar in the center of the actuator bearing frame using a cylinder that fits over the tibia and is fixed to the bone using polyester resin (Motip Dupli B.V., The Netherlands). Rotation around the longitudinal axis is blocked by a screw, which results in a system for the simulated knee that allows horizontal translation in the step direction and rotation in the sagittal plane only. A linear guiding system with servo electric motor and encoder (Bosh Rexroth AG, type MSK061C, Bosch Group, Germany) drives the foot bearing frame to simulate the horizontal

Table 1. Relevant dimensions of the different feet for use in the model for generating the tibial kinematics control input.

Foot number	Leg length (l)	Foot length (b)	Ankle height (a)	Ankle-heel-distance (q)	Toe-ankle-distance (r)
1	560	190	60	45	145
2	510	180	70	45	135
3	510	180	60	40	140
4	520	200	70	55	145
5	550	180	65	50	130
6	535	195	80	45	150
Mean	531	188	68	47	141
Std	21	9	8	0.5	7

All parameters are in millimeters.

Figure 1. Diagram of the gait simulator with the front part removed. The simulator features a framework, carrying the actuator bearing frame. The actuators apply loads to a foot, mounted in the center of the actuator bearing frame. A sliding carriage, driven by a servo electric motor, drives the foot through the stance phase of gait. The details on the right show the chain from actuator to tendon clamp.
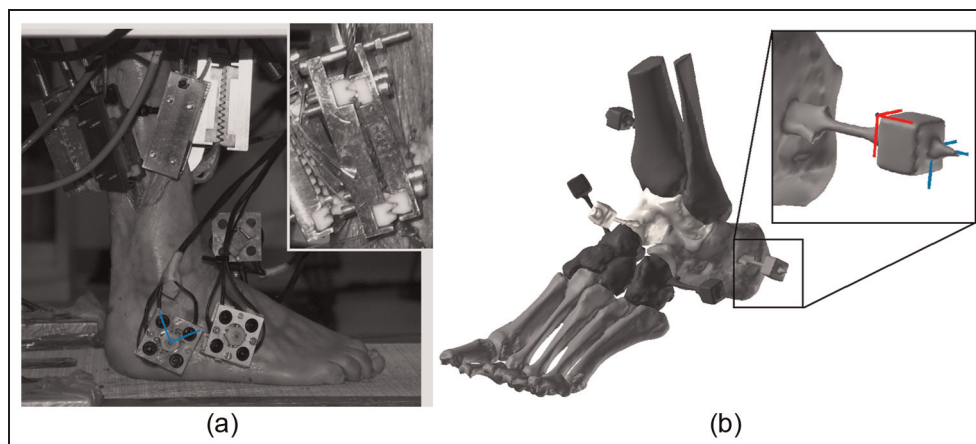
Figure 2. (a) The foot mounted in the gait simulator. Custom-built clamps are attached to the tendons of the six muscle groups. A detail of one clamp is shown in the top right of the left image. The marker clusters, from which three are visible, are also present, with the cluster-related technical coordinate frame indicated. (b) The 3D bone reconstruction from the CT data of the foot with pins is shown. A detail of one pin with the cube mounted on it is shown on the top right, with the cube-related and cluster-related technical coordinate frames indicated.

progression of the tibia through stance. A matching Indradrive® controller (Bosh Rexroth AG, type HCS02.1E, Bosch Group, Germany) controls the simulated knee position. Using a digital inclinometer (Solatronic, Fisco Tools Ltd, UK), mounted on top of the actuator bearing frame, the tibia-ground angle at heel contact was controlled to 14° by manually tilting the actuator bearing frame, with the foot mounted in a slight abducted position by rotating the tibia a few degrees outward. This mounting position was visually inspected by verifying the angle between the medial foot border and the forward progression direction of the actuator bearing frame.

The actuators, equipped with proportional valves and pressure sensors (Festo AG & Co. KG, Germany), apply load to six distinctive muscle groups. The loading capacity of the actuators was determined based on the scaled force magnitudes calculated using the static optimization for the gait cycle of one test subject, as explained further under the protocol subsection. They are 400 N for the combined Mm. peronei and the M. tibialis posterior, 200 N for

the M. flexor hallucis longus and M. flexor digitorum longus, 1000 N for the pretibial muscles (i.e. combined M. extensor hallucis longus, M. extensor digitorum longus, and M. tibialis anterior), 2750 N for the M. triceps surae, and 550 N for the vertical ground reaction force (vGRF).

A load cell (Vishay Tedea-Huntleigh, Vishay Electronic GmbH, Germany), in series with the actuator, measures the force applied to the tendons using custom-built nylon tendon clamps (design based on Tak-Man and Zhang[16]). The design of the clamps allows to apply high loads (1800 N) without slippage or rupture of the tendon. The integrity of the retinacula and other guiding structures ensures that the muscle line of action is maintained in the physiological configuration and the moment arm is not influenced by the clamp. A custom-built tensioning device connects the load cell and clamp to allow pretensioning of the chain between actuator and tendon.

The forces applied to the tendons are controlled through a force-feedback control mechanism: a proportional–integral–derivative (PID) control loop with hysteresis compensation controls the level of pneumatic pressure and therefore the applied force using the load cell output. Real-time data-processing and control is done on a Dell precision 390 (Dell, USA), running the Pharlab ETS real-time operating system (National Instruments, USA) and Labview programs (National Instruments, USA).

A force plate (Kistler multicomponent force plate, Kistler Instrumente GmbH, Germany) supports the foot. An actuator below the plate applies and modulates the vGRF by displacement control, fitting the measured vertical plate position to a target value, thereby driving the vertical position of the tibia.

Measurement devices

The motion of the bones that we inserted the intracortical pins (tibia, talus, calcaneus, navicular, and cuboid) is measured during gait simulations by a Krypton Optoelectronic Motion Capture System (Krypton K 600, Metris, Belgium), consisting of two camera modules, each containing three charge-coupled devices (CCDs). The cameras track the motion of five clusters, containing four active markers at a sampling frequency of 100 Hz. The clusters are mounted on a cube with known dimensions, screwed on the bone imbedded pins. System accuracy for tracking marker positions is 90 μm.

The force plate measures the GRF and ground moments at 1000 Hz. On top of the force plate, a pressure plate (Footscan system, 0.5 m with 3D interface box, RS Scan Int., Belgium) measures the plantar pressure distribution at 500 Hz for 0.8-s gait trials and at 75 Hz for 10-s gait simulations. All data are collected and synchronized by a 16-bit-resolution daqbook (Daqbook 2005, IoTech, USA).

Protocol

To determine control inputs, first, actuator force magnitudes (Figure 3) were calculated using a multibody simulation of a gait trial of a 47.9-kg, female control subject. Combining inverse analysis and static optimization as implemented in OpenSim,[17,18] individual muscle forces were calculated. Calculated muscle force time variation was compared with available surface electromyography (EMG) signals of the superficial muscles or published muscle timing sequences to validate the optimization results.[19] These model forces were linearly downscaled by a factor of 2 to ensure cadaveric integrity throughout the testing. The resulting force magnitudes correspond to a simulated body weight (BW) of 25 kg. Before testing, these actuator forces were then minimally tuned (up to a maximum of 10%) for each foot when necessary to obtain a normal plantar pressure distribution over the complete stance phase as well as normal ankle-foot kinematics. More specific, heel strike on the lateral calcaneus, gradual forefoot loading, followed by gradual heel lift were verified.[5] Once defined, these forces were unchanged in all consecutive tests.

Second, the control input imposing the horizontal translation of the tibia was derived from the horizontal translation of the knee marker during a representative gait cycle of the control subject, measured using a 3D motion capture, and was scaled to the dimensions of the lower leg by a factor, given by the following equation (Figure 3)

$$\text{Scale factor} = \frac{c'}{c} \text{ with } c'$$

$$= q + \sqrt{l^2 + q^2 - (1 + q \cdot \tan\alpha)^2 (\cos\alpha)^2}$$

that is, the ratio of the horizontal distance the simulated knee axis travels until midstance as a function of foot and gait parameters (c′) and the distance the knee travels until midstance for the control subject (c). In this equation, l is the leg length, measured as the distance between the simulated knee joint axis and the foot sole with the foot positioned as during upright standing, q is the horizontal distance between the back of the heel and ankle joint axis, and α is the angle between the shank axis and the line perpendicular to the ground.

Finally, vertical displacement of the force plate, dictating the relative vertical displacement between knee and ground, was calculated from the horizontal knee displacement combined with a model of sagittal plane motion of the shank and foot, illustrated in Figure 3.[8] It takes into account the lower leg length (l), the total foot length (b), measured as the distance between the back of the heel and the head of metatarsal one, the horizontal distance between the heel and the lateral malleolus (q), and the vertical distance between the lateral malleolus and the floor (a).

The experimental protocol started with a static trial with the foot as in normal upright standing and loaded
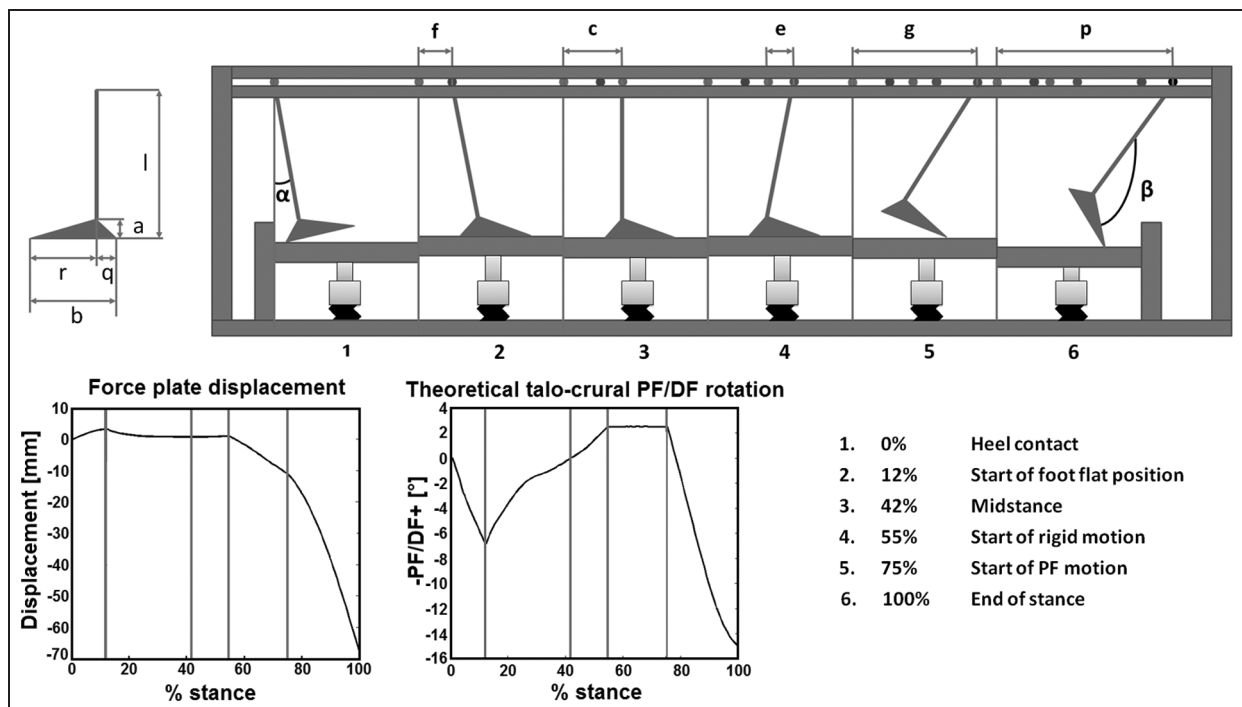
Figure 3. Illustration of the model used to generate the tibial kinematics control input. The foot starts in a 90° position at heel contact and then moves toward a foot flat position after which the simulated knee moves over the ankle. Subsequently, there is a rigid body phase and eventually a plantarflexion motion until push off. The vertical force plate displacement is shown on the bottom left, together with the theoretical sagittal talo-crural joint rotation. Inputs to the model are the foot dimensions, shown on the top left, the initial angle between the shank and the line, perpendicular to the ground (α), and the final amount of PF, expressed by the angle between the shank and the foot (β).
PF: plantarflexion; DF: dorsiflexion.

with the simulated BW (25 kg, i.e., 245 N). This foot position was used as a reference for bone kinematics, defining the zero-degree angular position. Thereafter, we collected 10 trials of normal walking per specimen with a stance phase duration of 10 s.

Data analysis

In order to quantify device performance, a regression analysis between the set points and measured control inputs was performed.[1] R^2 values, slope S of the regression line, and the root mean-squared error (RMSE) were calculated and averaged over all measurements within each session of 10 trials. R^2 values and S close to one together with low values for the RMSE reflect good apparatus control.

The 3D joint kinematics was calculated by quantifying the relative motion between the anatomical coordinate frames of each bone combination that forms an articulation. The kinematics reflects the positional difference of the distal bone in relation to the proximal one. Landmarks defining the anatomical frame are listed in Table 2. The landmarks define a plane of the coordinate frame, with the third frame axis perpendicular to it. The planes of the local coordinate frames correspond to the anatomical planes of the respective joints: motion in the sagittal plane is referred to as plantarflexion and dorsiflexion, motion in the frontal plane

is referred to as inversion and eversion, and motion in the transverse plane is referred to as abduction and adduction.

Relative motion of these frames was calculated by combining the recorded cluster movement and CT data of the bone pin assembly (Figure 2). Therefore, three consecutive transformations were combined. The first transformation between the technical coordinate frame, related to the titanium cube on which the led cluster is mounted, and the anatomical coordinate frame is calculated using a custom-implemented user interface that allows defining both anatomical and technical coordinate frames on the 3D surface reconstruction of the bone. The second transformation between the cube-related technical frame and the led cluster-related technical frame is known from the design of the assembly of both parts. The third transformation between the marker cluster-related technical frame and the global coordinate frame is calculated from the measured motion of the led clusters in the global coordinate frame. Combining these consecutive transformations allowed to reconstruct the position of the bones in the global coordinate frame and therefore to quantify the relative motion between bones and thus joint kinematics.

Joint kinematics is represented by joint rotations and translations. Rotations are represented by Euler angles (sequence sagittal (z), frontal (x), and transverse (y) plane motions), calculated in a similar way as Lundgren

Table 2. Landmarks for anatomical coordinate frame definition for the different bones. The frame is constructed using the landmarks such that the frame axes are in the anatomical planes of the respective joints. The landmarks define a coordinate plane, with the third axis perpendicular to it. The table also lists the origin of the frame, whose motion in the distal anatomical coordinate frame is the joint translation that was calculated.

Bone	Origin	Landmark 1	Landmark 2	Landmark 3
Tibia	Point halfway medial and lateral malleolus	Medial malleolus	Lateral malleolus	Point on central axis of fibula
Talus	Tip of the posterolateral tubercle	Center of the talar head	Tip of the lateral process	Tip of the posterolateral tubercle
Calcaneus	Point between lateral and medial tuberosity on the inferior surface	Sinus tarsi (intersection of the bifurcate ligament)	Point between lateral and medial tuberosity on the inferior surface	Point on the anterior tuberosity of the inferior surface
Cuboid	Most posterior point on the anterior border of the dorsal surface	Most anterior point on the anterior border of the dorsal surface	Most posterior point on the anterior border of the dorsal surface	Most plantar point of the inferior border of the posterior surface
Navicular	Center of the navicular cup	Center of the navicular cup	Tip of the medial border of the dorsal surface	Tip of the lateral border of the inferior surface

Table 3. Parameter values quantifying device performance, obtained through regression analysis between the set points and measured control inputs.

	Mm. Peronei	Pretibial muscles	M. tibialis posterior	M. flexor hallucis longus	M. triceps surae	M. flexor digitorum longus	Force plate displacement
R^2	0.99 (0.00)	0.99 (0.00)	0.97 (0.04)	0.39 (0.33)	1.00 (0.00)	0.20 (0.24)	0.95 (0.02)
S	0.98 (0.01)	1.01 (0.03)	0.97 (0.02)	0.39 (0.50)	1.01 (0.00)	0.18 (0.40)	1.13 (0.07)
RMSE	4.43 (1.14)	11.89 (1.61)	4.47 (1.57)	0.74 (0.26)	15.57 (6.17)	0.69 (0.28)	2.24 (0.73)

RMSE: root mean-squared error.
R^2 and S are dimensionless parameters.
RMSE is expressed in Newton for forces and in millimeter for the force plate displacement.

et al.[20] in order to ease the comparison between our results and the golden standard for in vivo foot kinematics. In contrast to Lundgren et al., landmark-based anatomical coordinate frames are defined, with their relative motion representing bone kinematics. This approach mainly reflects anatomy-dependent variability in kinematics and is therefore expected to give better interspecimen repeatability. This could improve the ability to draw general conclusions on gait kinematics, valid for a more global population of feet. Translations were calculated as the displacement of the origin of the distal anatomical coordinate frame along the axes of the proximal anatomical coordinate frame. Data were normalized to 0%–100% of stance. Joint kinematics was corrected for the joint position measured during the static trial by subtracting the rotations and translations measured during this trial from those measured during the gait simulations. Kinematic data from the 10 trials were averaged for each specimen.

In order to quantify the reproducibility of our setup in subsequent trials, repeatability of the kinematic data and measured inputs to the control mechanism was quantified by the coefficient of multiple determination (CMD).[21] A value of 1 indicates exact repeatability of motion patterns. Furthermore, the SDs of all samples at a specific time instant in the stance phase were calculated and averaged over the complete stance phase as a measure of absolute variability.

In order to investigate the correspondence of our gait simulations to in vivo conditions, we first calculated the range of motion (ROM) of joint rotations and translations and compared it with the golden standard for in vivo kinematics[20] and the results of the most recently published in vitro study on foot kinematics,[7] where possible. Next, we calculated the CMD between the average of the 10 repeated trials and the average in vivo data[20] for each specimen in order to quantify the correspondence of the simulated motion patterns to those in vivo.

Results

Figure 4 shows the quality of the control performance. It displays a good agreement between the set points and the applied inputs as well as a narrow confidence band for the latter. This observation is confirmed by the R^2 values, S, and RMSE (Table 3) which reflect high control performance. R^2 values are above 0.9 and S is close to one for most muscle actuators and the force plate displacement control. Also the RMSE is acceptable with a maximum of 15.57 N for the M. triceps surae, which is only 1.3% of the maximal force during stance. Although slightly higher when taking into account the limited maximal force magnitudes of 7 and 8 N for the M. flexor hallucis longus and M. flexor digitorum longus, respectively, the RMSEs of 0.74 and
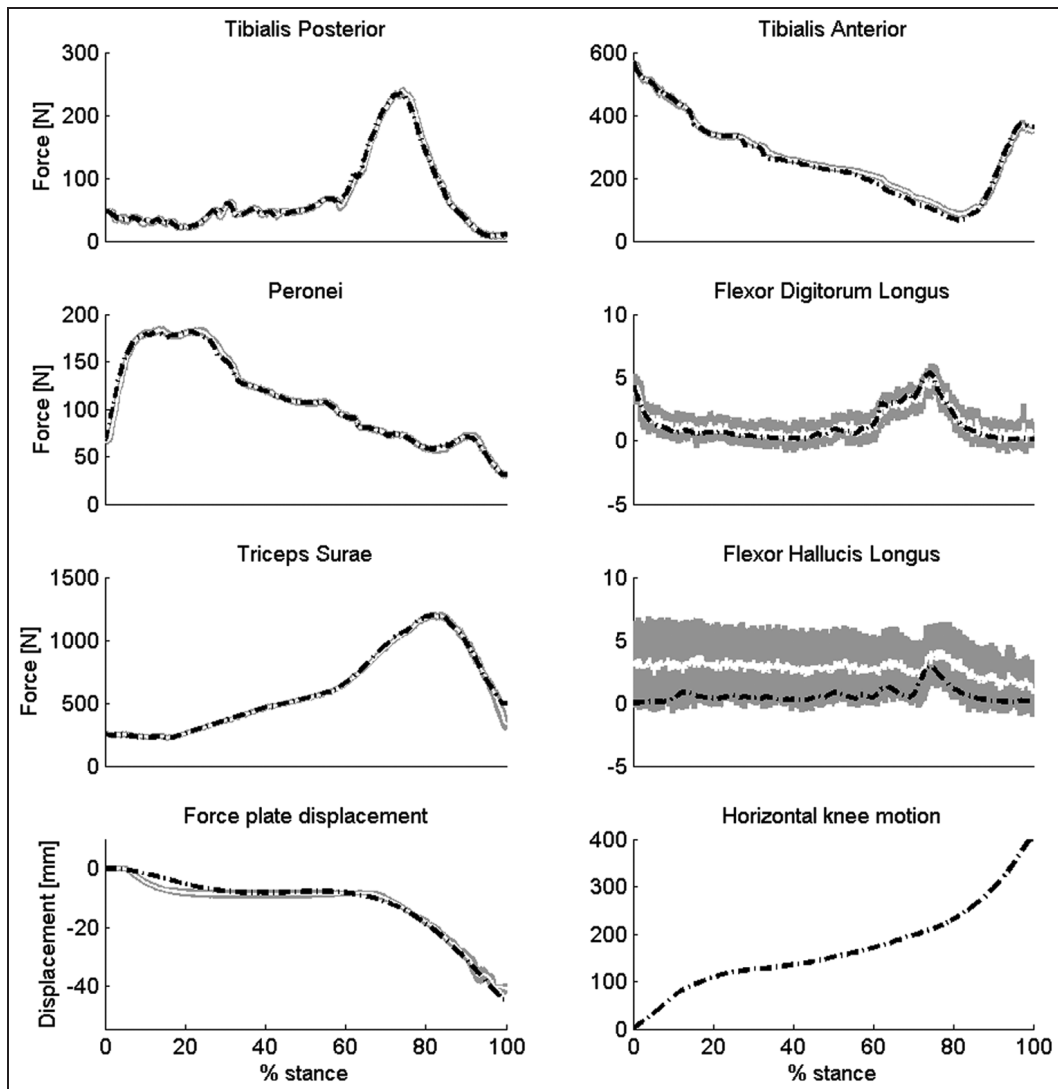
Figure 4. Set points and measured control inputs for one foot. Set points are indicated by the black dashed lines, measured control inputs are represented by solid white lines, and the SD in gray, representing control input variability in consecutive tests. Set points were only slightly different for the other feet tested as forces were fine tuned until a normal gait pattern and plantar pressure pattern were obtained.

0.69 N are low. Also the force plate position is accurately controlled with an average RMSE of 2.24 mm.

Table 4 shows the repeatability of these inputs. It reflects high repeatability as CMD values are close to one and the SD is limited when compared with the range of the inputs. A maximum SD of 15.64 N is reported for the M. triceps surae, being only 1.3% of the maximum applied force during simulation. Although slightly higher relative to the range, the SDs for M. flexor hallucis longus and M. flexor digitorum longus are limited to 1.47 and 2.55 N, respectively.

Figure 5(a) and (b) presents the average joint rotations and translations during stance over the 10 trials for each foot. In addition, Figure 5(a) compares joint rotations with the golden standard for in vivo joint kinematics[20] and the in vitro results of Whittaker et al.[7] As reflected by these curves, there is a good interspecimen repeatability. In addition, there is a good correspondence with in vivo and in vitro kinematics of Lundgren et al.[20] and Whittaker et al.,[7] despite some deviations for rotations in the frontal and sagittal plane at the calcaneocuboid and talo-navicular joints. This is confirmed in Table 5, which compares the ROM for our data with that of Lundgren et al.[20] and Whittaker et al.[7] and displays the CMD between our in vitro measured motion patterns and those measured in vivo.[20] Although slightly reduced, the ROM for our data is comparable with that in vivo, in particular, for the tibio-calcaneal and tibio-talar joints, where the data of Whittaker et al. displays a somewhat increased ROM compared with in vivo. In addition, we observe the highest ROM at the different joints in the plane, where we also see the highest ROM in vivo. The CMD values reflect good correspondence between in vitro and in vivo motion patterns for the tibio-calcaneal, tibio-talar and talo-calcaneal, and talo-navicular joints. These

Table 4. Parameter values that quantify the variability of the control input (muscle forces and force plate displacement) and output (joint rotations, vGRF, and COP displacement).

	CMD		Average SD over stance
	In vitro	In vivo	In vitro
Mm. Peronei	0.96 (0.08)		4.03 (2.06)
Pretibial muscles	0.99 (0.01)		9.39 (4.32)
M. tibialis posterior	0.99 (0.01)		3.17 (1.72)
M. flexor hallucis longus	0.43 (0.34)		1.47 (1.82)
M. triceps surae	1.00 (0.00)		15.64 (6.05)
M. flexor digitorum longus	0.09 (0.06)		2.55 (1.55)
Force plate displacement	0.95 (0.07)		1.31 (0.34)
vGRF	0.70 (0.12)		62.50 (9.96)
COP—medio-lateral position	0.83 (0.08)		3.27 (0.89)
COP—anterior-posterior position	0.97 (0.02)		9.42 (1.46)
Tibia-calcaneus—frontal plane	0.68 (0.31)	0.96 (0.02)	0.71 (0.43)
Tibia-calcaneus—transverse plane	0.77 (0.19)	0.98 (0.01)	0.50 (0.11)
Tibia-calcaneus—sagittal plane	0.80 (0.15)	0.97 (0.02)	1.51 (0.39)
Tibia-talus—frontal plane	0.62 (0.33)	0.91 (0.04)	0.82 (0.92)
Tibia-talus—transverse plane	0.65 (0.30)	0.93 (0.06)	0.96 (0.88)
Tibia-talus—sagittal plane	0.76 (0.14)	0.98 (0.01)	1.57 (0.63)
Talus-calcaneus—frontal plane	0.52 (0.44)	0.91 (0.08)	0.92 (0.86)
Talus-calcaneus—transverse plane	0.62 (0.30)	0.93 (0.05)	0.44 (0.24)
Talus-calcaneus—sagittal plane	0.54 (0.38)	0.89 (0.12)	0.79 (0.47)
Talus-navicular—frontal plane	0.69 (0.33)	0.98 (0.01)	1.63 (0.69)
Talus-navicular—transverse plane	0.66 (0.37)	0.95 (0.07)	1.78 (1.06)
Talus-navicular—sagittal plane	0.49 (0.39)	0.94 (0.06)	1.12 (0.52)
Calcaneus-cuboid—frontal plane	0.80 (0.12)	0.91 (0.07)	0.94 (0.35)
Calcaneus-cuboid—transverse plane	0.75 (0.21)	0.86 (0.08)	0.94 (0.67)
Calcaneus-cuboid—sagittal plane	0.66 (0.33)	0.86 (0.03)	0.35 (0.22)
Navicular-cuboid—frontal plane	0.91 (0.04)	0.91 (0.05)	0.42 (0.12)
Navicular-cuboid—transverse plane	0.73 (0.28)	0.87 (0.09)	0.73 (0.65)
Navicular-cuboid—sagittal plane	0.41 (0.35)	0.90 (0.06)	0.41 (0.31)

CMD: coefficient of multiple determination; COP: center of pressure; vGRF: vertical ground reaction force.
The CMD reflects repeatability of motion patterns and is dimensionless.
For comparison, the intraspecimen variability of in vivo kinematics is reported.[12]
The SD of the output, averaged over stance, is shown to reflect the absolute magnitude of variability.
SD is in Newton for forces, in millimeter for COP and force plate displacement, and in degrees for the joint rotations.
Average values are reported with the SD in brackets.

values are comparable with those that reflect the correspondence between the data of Whittaker et al.[7] and Lundgren et al.[20] This reflects similar correspondence of our data to that of Lundgren et al. as for the data of Whittaker et al., and even better correspondence of our data for the transverse plane rotations at the tibio-calcaneal, talo-calcaneal, and talo-navicular joints. For the calcaneocuboid and navicular-cuboid joints, these values reflect the discrepancy between in vitro motion patterns and those in vivo, in particular at the beginning and end of stance. There is no data of Whittaker et al. that allows further comparison.

The repeatability of these data as reflected by the CMD is acceptable when compared with the intrasubject variability that is observed in vivo (Table 4). Values are lower than in vivo, yet still reflecting good repeatability (always above the level of 0.5), except for sagittal talo-navicular and navicular-cuboid rotations. The SD values are never above 2° on average, indicating good repeatability of joint kinematics.

Figure 6 shows the average vGRF and center of pressure (COP) motion in individual feet. We observe the typical M-shape in all but one foot. However, force magnitudes are larger than in vivo for the simulated BW (up to double what is expected during in vivo gait[22]). For the COP displacement, the typical pattern of anterior-posterior and medio-lateral motion is observed in all but one foot.

Discussion

Since the first publication on dynamic, cadaveric gait simulation,[1] there have been new developments by multiple groups over the world. Many limitations have been eliminated in subsequent designs, being mainly the limited degrees of freedom of the mechanism controlling the kinematics of the tibia, the low gait speed, the limited forces applied to the tendons, and the limited ground reaction force magnitudes. However, specific problems still remain to be solved, one being the lack of specimen specificity of the inputs to the control mechanism of the gait simulator, in particular of those inputs that define the tibial kinematics.[1,7] Therefore, we developed a new gait simulator that extends performance of current state-of-the-art simulators in the following aspects: first, in our setup, the applied tendon

Table 5. Quantitative comparison of the in vitro gait simulations and in vivo gait data.

	Tibia-calcaneus			Tibia-talus			Talus-calcaneus			Talus-navicular			Calcaneus-cuboid			Navicular-cuboid		
	Front	Trans	Sag	Front	Trans	Sag	Front	Trans	Sag	Front	Trans	Sag	Front	Trans	Sag	Front	Trans	Sag
ROM—in vitro rotations	5.8 (3.0)	5.0 (2.0)	16.2 (5.4)	3.6 (1.6)	5.8 (1.5)	13.2 (5.4)	4.9 (3.9)	2.8 (1.1)	4.5 (3.1)	14.6 (5.8)	14.1 (6.5)	5.5 (4.0)	7.2 (1.2)	6.7 (1.6)	2.2 (1.0)	5.3 (1.9)	4.0 (1.0)	1.6 (0.8)
ROM—in vivo rotations (Lundgren)	11.3 (3.5)	7.3 (2.4)	17.0 (2.1)	8.1 (3.8)	7.8 (2.7)	15.3 (2.0)	9.8 (1.8)	7.5 (2.0)	6.8 (1.4)	14.9 (6.1)	16.3 (6.5)	8.4 (1.1)	11.3 (3.9)	8.1 (2.0)	9.7 (5.2)	8.8 (4.4)	8.9 (4.3)	7.2 (2.4)
ROM—in vitro rotations (Whittaker)	9.2 (3.0)	10.7 (3.6)	23.6 (7.0)	6.2 (3.8)	11.0 (6.5)	23.2 (4.6)	8.6 (5.2)	6.2 (2.3)	6.8 (1.9)	18.8 (4.8)	14.9 (5.5)	9.6 (4.6)	8.6 (0.5)	7.5 (1.8)	8.8 (1.9)	4.9 (3.0)	20.1 (11.1)	18.7 (9.4)
ROM—in vitro translations	11.82 (4.11)	13.06 (5.99)	5.74 (1.72)	2.45 (1.53)	6.03 (2.40)	3.82 (1.63)	3.23 (2.82)	2.49 (1.60)	3.84 (2.24)	1.34 (0.59)	1.19 (0.60)	1.08 (0.47)	0.71 (0.18)	1.08 (0.26)	1.43 (1.02)	1.55 (0.32)	1.16 (0.29)	0.75 (0.26)
CMD—in vitro vs Lundgren	0.68 (0.22)	0.56 (0.16)	0.89 (0.06)	0.52 (0.32)	0.52 (0.17)	0.84 (0.07)	0.60 (0.21)	0.65 (0.18)	0.67 (0.11)	0.60 (0.25)	0.61 (0.18)	0.66 (0.10)	0.44 (0.45)	0.41 (0.43)	0.65 (0.17)	0.53 (0.15)	0.54 (0.31)	0.36 (0.16)
CMD—Whittaker vs Lundgren	0.98	0.15	0.94	–	–	0.95	0.85	0.19	0.67	0.97	0.41	0.76	0.73	–	0.92	–	–	–

ROM: range of motion; CMD: coefficient of multiple determination.

The top rows present the range of motion (ROM) of the joint rotations (degrees) and translations (mm) measured.

The ROM of joint rotations is compared with the ROM of the golden standard for in vivo kinematics[20] and the ROM that was observed in the most recent in vitro study on joint kinematics during stance.[7]

The bottom rows present the CMD between the mean of 10 in vitro gait simulations and the mean of the in vivo data of Lundgren et al.[20] and the in vitro data of Whittaker et al.[7].

Values are averages with the SD in brackets.

forces are calculated using an inverse dynamics approach and static optimization. In contrast to other groups that use information on EMG muscle activation and the average cross-sectional area of the muscles and their maximal force generating capacity, our approach calculates a set of muscle forces that minimizes the difference between joint and muscle moments while minimizing overall muscle activity level. This approach accounts for the muscle force length and velocity dependency that cannot be accounted for if EMG is scaled to the maximal force generating capacity of the muscle. Second, the methodology for controlling tibial kinematics eliminates the need for manual and arbitrary tuning of the horizontal and vertical knee translation. In addition, it solves the problem of generating good tibial kinematics control inputs for simulations with feet, having more extreme dimensions.[1,7] Third, we present a strategy to calculate complete 3D joint kinematics. It is unique as the combined use of CT data with data from a 3D motion capture device allows extending the currently available data on joint rotations of selected foot bones[9–14] with joint translations that were not previously documented. These additional data are relevant for a profound validation of numerical models and for gaining more insight in foot biomechanics.

Our setup achieves very high control performance and repeatability of the inputs. Only two muscles with relatively low forces (M. flexor digitorum longus and M. flexor hallucis longus) show smaller values for R^2 and S compared with the other muscles. However, as their force magnitudes are only slightly higher than the measurement noise of the load cells, these parameters are bad indicators of control performance for these muscles, as the absolute deviation between the set point and applied force is small. The observed errors for the applied muscle forces will have very limited effects on joint kinematics and kinetics. It can therefore be concluded that all input parameters to the setup are well controlled and allow repeatable simulations of the stance phase of gait.

The measured hindfoot kinematics show acceptable correspondence to the golden standard for in vivo kinematics and kinetics,[20] comparable with the correspondence of published in vitro data[7] and even better for transverse plane rotations of the joints that were included in this study. This implies that the presented approach allows simulations with bone rotations in different planes, representative of normal gait. The most significant deviations were seen in the transverse plane for the talo-navicular and calcaneocuboid joints, which present opposite patterns compared with in vivo. This was also seen for rotations at the tibio-calcaneal joint for some feet that relates to the elevated vGRF as discussed hereafter.

For the vGRF and COP, we observed the typical change of force and position over stance in most feet. Only in one foot, increased midfoot loading was achieved during simulation, therefore shifting the COP
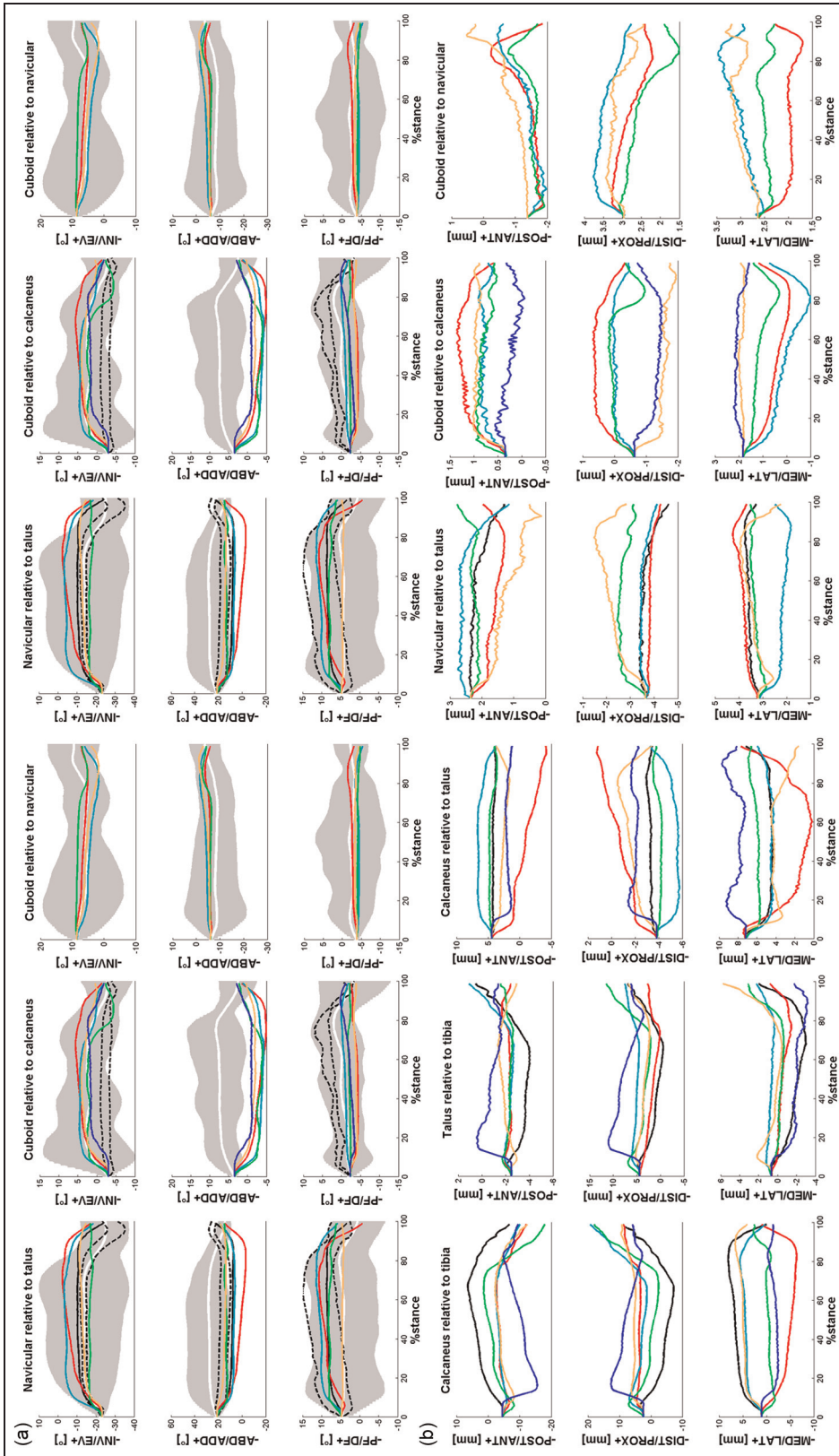
Figure 5. (a) Average hindfoot rotations of the six feet measured, represented by the solid lines, compared with the golden standard for in vivo kinematics, [20] represented by the solid white line and interspecimen SD in gray, and compared with the most recent in vitro dynamic gait simulation results, [7] for which the confidence interval is represented by the dashed black lines. The difference in offsets of the curves is eliminated by calculating the mean initial offset of all feet tested and shifting all curves to have the same rotation angle at heel contact in order to ease the comparison of motion patterns, as was done before. [7] (b) Average hindfoot translations of the six feet measured. The difference in offsets of the curves is eliminated by calculating the mean initial offset of all feet tested and shifting all curves to have the same translation value at heel contact in order to ease the comparison of motion patterns, as was done before. [7]

PF: plantarflexion; DF: dorsiflexion; ABD: abduction; ADD: adduction; INV: inversion; EV: eversion; MED: medial; LAT: lateral; DIST: distal; PROX: proximal; POST: posterior; ANT: anterior.
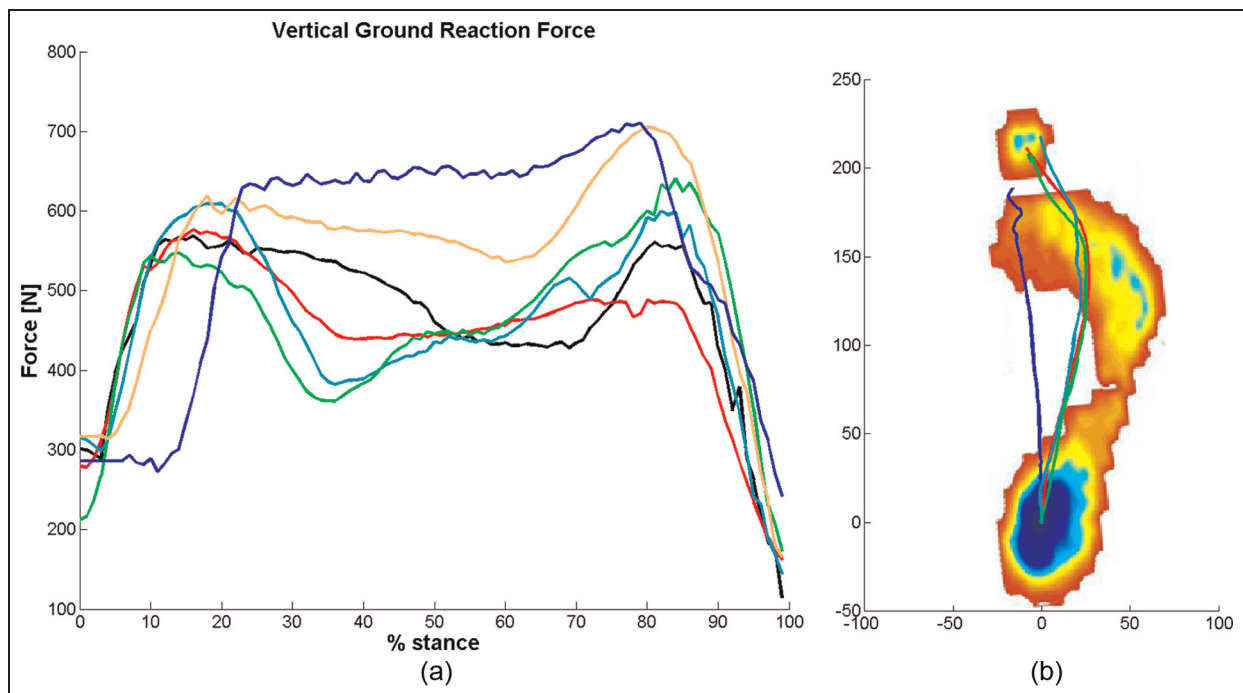
Figure 6. Kinetic results: (a) the vertical ground reaction force for all feet tested and (b) the COP displacement for four of the six feet, as data for two feet was corrupted during the measurements. COP position is measured in millimeters.

immediately from the heel to the first metatarsal. In this foot, also the decrease of the vGRF at midstance is seen to be absent. Furthermore, one can observe abnormal ankle kinematics with a high initial plantarflexion at the ankle, followed by a limited motion into dorsiflexion and only limited plantarflexion at the end of stance. These abnormalities can be explained by an elevated tibia-ground angle (α in Figure 3) at initial contact compared with the one assumed by the model in Figure 3. Such an elevated tibia-ground angle will increase the slope of the foot with respect to the ground at heel contact and thus initial plantarflexion. At midstance, such an elevated angle would require the force plate to drop more. If not, this results in an increased vGRF and decreased dorsiflexion. This stresses the importance of a correct initial inclination of the tibia with respect to the ground at initial contact. A newer version of our gait simulator includes a mechanism that ensures the correct and repeatable positioning of the specimen at the beginning of the stance phase, in order to avoid such complications.

Despite the corresponding pattern of the vGRF with curves observed in vivo, we need to acknowledge that the magnitude of the vGRF is considerably higher than in vivo for the simulated BW. This is a consequence of slight inaccuracies in the control of force plate position (2.24 mm on average), which results in additional compression of the leg and foot. Due to the high structural stiffness of the leg and foot in the setup, this limited additional compression results in a considerable increase in the vGRF. However, as the error with respect to the desired position of the force plate is

small, the effects on the kinematics in the sagittal plane are limited. On the other hand, this can explain the unexpected motion into abduction at the talo-navicular and calcaneocuboid joints. In order to further normalize the magnitude of the vGRF and associated kinematics, enhancement of the control of the force plate is currently being implemented.

Although the current results clearly demonstrate the ability to induce hindfoot kinematics comparable with previously published data with typical vGRF and COP patterns, some additional aspects need to be acknowledged. First, the applied muscle force magnitudes are below the physiological magnitudes observed in a normal adult population.[23] However, as cadaver integrity is of prior concern, forces are kept low, as is the case in all studies where dynamic in vitro experiments were performed.[9–14] As a consequence, there is a decrease in the ROM, and load transfer in the joints will be reduced, which means intra-articular pressures are reduced compared with in vivo. In contrast, motion patterns remain largely unaffected as the main muscle action remains unaffected. Second, also gait speed and acceleration are reduced compared with in vivo, as was also the case in previous studies.[9–14] However, as bones in the foot are small, the resulting forces of inertia will be small compared with the muscle forces and ground reaction forces. Consequently, there is limited impact of these reduced forces of inertia on bone motion. On the other hand, there might be an effect on the viscoelastic behavior of the ligaments and other soft tissues and on the intra-articular pressures. However, previous studies have shown that experiments with clinical relevance are

still possible despite these limitations.[9–14] Third, there is an oversimplification in the model to generate input signals for controlling the tibial kinematics. In particular, we assume the knee and ankle joint axis to be fixed and all segments to be rigid. Furthermore, the setup has limited degrees of freedom to control knee movement as is the case in existing gait simulators.[1,3–5] In particular, our setup lacks to simulate the frontal and transverse plane motion that occurs at the knee and which was observed to be quite crucial.[24] However, as for the reduced forces, our results have shown that kinematics similar to in vivo can still be achieved despite these simplifications.

Other factors relate to aspects, common in all existing gait simulators, that is, the lack of activation of intrinsic foot musculature, altered soft tissue properties when compared with in vivo, the lack of neuromuscular control, and the lack of knowledge on specimen-specific muscle forces (which requires arbitrary tuning of these control inputs). Consequently, it is not possible to exactly reproduce the kinematics of the living subject for a particular specimen.

Despite these limitations, the correspondence of the kinematics and kinetics with in vivo data for a sample of specimens with varying dimensions shows the relevance and validity of including specimen-specific information for defining the control inputs. More specifically, this approach eliminates the need for arbitrary editing of the input for controlling tibial kinematics. In addition, it provides us with data that show comparable correspondence with in vivo data[20] as that of the most recent data of in vitro gait simulations,[7] and even better correspondence for the transverse plane rotations, despite the limited amount of degrees of freedom for controlling tibial kinematics in the presented setup. Therefore, the setup provides opportunities to evaluate the quality of numerical model predictions of the motion patterns for a particular specimen, to investigate the kinematic and kinetic behavior of implants and to perform clinical studies, similar to those presented in the literature.[9–14]

Conclusion

We have developed a setup for dynamic in vitro gait simulation, integrating a unique approach for generating the tibial kinematics control input. In addition, we presented a methodology to reconstruct complete 3D joint kinematics, that is, both rotations and translations, and we presented these kinematic results for the tarsal joints in the foot. The setup has good control performance and gives repeatable kinematics, vGRF, and COP displacement, with the most important motion patterns comparable with in vivo.

Acknowledgements

Declaration of conflicting interests

The authors declare that there are no conflicts of interest.

Funding

References

1. Sharkey N and Hamel A. A dynamic cadaver model of the stance phase of gait: performance characteristics and kinetic validation. *Clin Biomech* 1998; 13: 420–433.
2. Nester CJ. Lessons from dynamic cadaver and invasive bone pin studies: do we know how the foot really moves during gait? *J Foot Ankle Res* 2009; 2: 18.
3. Kim K, Kitaoka H, Luo Z, et al. In vitro simulation of the stance phase of human gait. *J Musculoskelet Res* 2001; 5: 113–121.
4. Hurschler C, Emmerich J and Wulker N. In vitro simulation of the stance phase gait part 1: model verification. *Foot Ankle Int* 2003; 24: 614–622.
5. Nester C, Liu A, Ward E, et al. In vitro study of foot kinematics using a dynamic walking cadaver model. *J Biomech* 2007; 40(9): 1927–1937.
6. Noble LD, Colbrunn RW, Lee D, et al. Design and validation of a general purpose robotic testing system for musculoskeletal applications. *J Biomech Eng: T ASME* 2010; 132(2): 025001.
7. Whittaker EC, Aubin PM and Ledoux WR. Foot bone kinematics as measured in a cadaveric robotic gait simulator. *Gait Posture* 2011; 33: 645–650.
8. Natsakis T, Peeters K, Burg J, et al. Specimen specific tibial kinematics model for in vitro gait simulations. *J Eng Med* 2013; 4: 454–463.
9. Bayomy AF, Aubin PM, Sangeorzan BJ, et al. Arthrodesis of the first metatarsophalangeal joint: a robotic cadaver study of the dorsiflexion angle. *J Bone Joint Surg* 2010; 92: 1754–1764.
10. Lee DG and Davis BL. Assessment of the effects of diabetes on midfoot joint pressures using a robotic gait simulator. *Foot Ankle Int* 2009; 30: 767–772.
11. Okita N, Meyers SA, Challis JH, et al. An objective evaluation of a segmented foot model. *Gait Posture* 2009; 30: 27–34.
12. Kim KJ, Uchiyama E, Kitaoka HB, et al. An in vitro study of individual ankle muscle actions on the center of pressure. *Gait Posture* 2003; 17: 125–131.
13. Suckel A, Muller O, Langenstein P, et al. Chopart's joint load during gait: in vitro study of 10 cadaver specimen in a dynamic model. *Gait Posture* 2008; 27: 216–222.
14. Meardon SA, Edwards B, Ward E, et al. Effects of custom and semi-custom foot orthotics on second metatarsal bone strain during dynamic gait simulation. *Foot Ankle Int* 2009; 30: 998–1004.

15. Imhauser C, Siegler S, Udupa J, et al. Subject-specific models of the hindfoot reveal a relationship between morphology and passive mechanical properties. *J Biomech* 2008; 41: 1341–1349.
16. Tak-Man J and Zhang M. A serrated jaw clamp for tendon gripping. *Med Eng Phys* 2006; 28: 379–382.
17. Lenaerts G, De Groote F, Demeulenaere B, et al. Subject-specific hip geometry affects predicted hip joint contact forces during gait. *J Biomech* 2008; 41: 1243–1252.
18. Delp SL, Anderson FC, Arnold AS, et al. OpenSim: open-source software to create and analyze dynamic simulations of movement. *IEEE T Biomed Eng* 2007; 54: 1940–1950.
19. Perry J. *Gait analysis: normal and pathological function.* Thorofare, NJ: Slack Inc., 1992.
20. Lundgren P, Nester C, Liu A, et al. Invasive in vivo measurement of rear-, mid- and forefoot motion during walking. *Gait Posture* 2008; 28: 93–100.
21. Kadaba MP, Ramakrishnan HK, Wootten ME, et al. Repeatability of kinematic, kinetic, and electromyographic data in normal adult gait. *J Orthop Res* 1989; 7(6): 849–860.
22. Sarrafian SK. *Anatomy of the foot and ankle* (chap. 10). Philadelphia, PA: J. B. Lippincott & Co., 1983, p.420.
23. Bogey R, Perry J and Gitter A. An EMG-to-force processing approach for determining ankle muscle forces during normal gait. *IEEE T Neur Sys Reh* 2005; 13: 302–310.
24. Belvedere C, Leardini A, Giannini S, et al. Does medio-lateral motion occur in the normal knee? An in-vitro study in passive motion. *J Biomech* 2011; 44: 877–884.

Appendix I

Notation

COP	center of pressure
GRF	ground reaction force
PID	proportional-integral-derivative
RMSE	root mean-squared error
ROM	range of motion
S	slope of the regression line in the regression analysis
vGRF	vertical ground reaction force
a	ankle height
b	foot length
c	distance the knee travels until midstance with vertical tibia for the control subject
c′	horizontal distance the simulated knee axis travels until midstance with vertical tibia
l	leg length
q	ankle-heel distance
r	toe-ankle distance
α	angle between the tibia and a line perpendicular to the force platform of the setup
β	angle between the tibia and foot sole
3D	three-dimensional
CCD	charge-coupled device
CMD	coefficient of multiple determination